

Design, Manufacturing, and Testing of Robo Raven

John Gerdes, Alex Holness, Ariel Perez-Rosado, Luke Roberts, Eli Barnett, Adrian Greisinger, Johannes Kempny, Deepak Lingam, Chen-Haur Yeh, Hugh A. Bruck, Satyandra K. Gupta¹

Technical Report, Advanced Manufacturing Lab, University of Maryland, College Park, MD 20742, April 2014

¹ Corresponding Author

Gerdes, J.W., Holness, A., Perez-Rosado, A., Roberts, L., Greisinger, A., Barnett, E., Kempny, J., Lingam, D., Yeh, C.H., Bruck, H.A., and Gupta, S.K., "Design, Manufacturing, and Testing of Robo Raven." Advanced Manufacturing Lab Technical Report, University of Maryland, College Park, April 2014.

Abstract

Most current bird-inspired flapping wing air vehicles (FWAVs) use a single actuator to flap both wings. This approach couples and synchronizes the motions of the wings while providing a variable flapping rate at a constant amplitude or angle. Independent wing control has the potential to provide a greater flight envelope. Driving the wings independently requires the use of at least two actuators with position and velocity control. Integration of two actuators in a flying platform significantly increases the weight and hence makes it challenging to achieve flight. We used our successful previous designs with synchronized wing flapping as a starting point for creating a new design. The added weight of an additional actuator required us to increase the wing size used in the previous designs to generate additional lift. For the design reported in this paper, we took inspiration from the Common Raven and developed requirements for wings of our platform based on this inspiration. Our design process began by selecting actuators that can drive the raven-sized wing independently to provide two degrees of freedom over the wings. We concurrently optimized wing design and flapping frequency to generate the highest possible lift and operate near the maximum power operating point for the selected motors. The design utilized 3D printed parts to minimize part count and weight while providing a strong fuselage. The platform reported in this paper, known as Robo Raven, was the first demonstration of a bird-inspired platform doing outdoor aerobatics using independently actuated and controlled wings. This platform successfully performed dives, flips, and buttonhook turns demonstrating the capability afforded by the new design.

1. Introduction

Unmanned aerial vehicles (UAVs) have gained a significant amount of attention in recent years due to their versatility in a wide variety of missions. UAVs may be broadly classified into rotorcraft, airplanes, and flapping wing air vehicles (FWAVs). Generally, rotorcraft are best suited for low speeds and hovering because of their excellent maneuverability but limited endurance. Airplanes are best suited for higher speeds and greater endurance, yet lack the maneuverability of rotorcraft. FWAVs may provide a versatile compromise between these two extremes while also offering safer and quieter operation due to reduced rotational speeds of lifting surfaces.

Biological inspiration is an important source of knowledge for the development of FWAVs. Research conducted by biologists into the aerodynamics, energetics, and morphology of flying birds has provided useful insight and design rules to designers of FWAVs [1-3]. Inspiration for flapping wing flight comes from the following three sources: bats, birds, and insects. Each of these creatures has unique flight characteristics.

Insects represent the smallest flying creatures, and thus their style of flight is uniquely adapted to their aerodynamic operating conditions. The tiny wings used by insects operate at very low Reynolds' numbers, and thus rely on unsteady aerodynamic effects to generate the required forces for flight [4]. Insects flap their wings very rapidly and thus are able to make corrective adjustments to their gait many times per second, leading to a high degree of control authority. This comes at the expense of large energetic demands. To cope with their high energy requirements for flight, insects rely on large powerful flapping muscles and elastic energy storage structures in their body, and their wings passively deform into airfoils due to the large loads imparted during rapid flapping motions [5]. Readers should refer to [4] for insect flight mechanics.

Bats represent an interesting style of flight, in that they operate at a size scale that is similar to many birds, yet they lack the tails that aid birds in maneuvering and stability. Interestingly, across a substantial range of sizes, bats tend to exhibit invariant wing kinematics for producing lift and thrust. In general, bats have a style of flight that more closely resembles birds, with increased emphasis on aerodynamic lift generation from forward motion, rather than the hovering exhibited by insects. Readers should refer to [6] for bat flight mechanics and [7] for a bat-inspired flying platform.

This paper is focused on avian-inspired FWAVs. Birds in general operate at significantly higher Reynolds' numbers. In addition, birds use their tails to augment stability and aid in maneuvers. Avian flight relies on more direct control over the shape of the wings achieved through muscular intervention. While insects passively deform their wings, birds have sophisticated muscular structures and feather control that allow for many degrees of freedom through wing morphing and folding, as well as 3D flapping patterns. The hummingbird is an interesting contradiction to this convention, as it is a bird that exhibits a more insect-like style of flight [8].

We are interested in developing a platform that can be used to investigate outdoor aerobatics maneuvers, so we decided to take inspiration from the Common Raven, a relatively large bird capable of aerobatics. Moreover, we want to provide customizable flapping motions, where each wing is powered with a separately controlled independent drive train, consisting of a motor, gears, position sensor, and feedback control loop. The benefit of this approach is to allow completely arbitrary wing motions, which provides increased freedom to explore some aggressive and interesting maneuvers. These include asymmetric roll initiation, upflap-downflap asymmetry, gliding and soaring dynamics, gust rejection, and blending of tail and wing steering modes.

In prior work, we have demonstrated the utility of FWAVs as research platforms and as practical flying prototypes capable of transmitting live video, morphing wings, large payload capacities, and recharging batteries using integrated flexible solar panels [9-20]. In the present effort, we apply many of the techniques previously developed to characterize and understand our design choices in detail. The results culminate in a flying prototype vehicle we call Robo Raven, a FWMAV that overcomes the substantial challenge of producing sufficient lift and thrust for sustained flight with fully independent wing control.

2. System Overview

2.1 Design Requirements

Our primary objective was to build a FWAV that can be used to learn about the effect of changing wing kinematics while improving the maneuverability of flapping wing air vehicles outdoors. So we sought to build a bigger platform that gives us the ability to control the position and velocity of each wing independently. Our efforts were inspired by the Common Raven, *Corvus Corax*, with properties listed in Table 1.

Table 1 – Properties of the Common Raven, *Corvus Corax* [21]

Parameter	Common Raven	Unit
<i>Total Mass</i>	0.69-2.00	kg
<i>Length</i>	0.63	m
<i>Wingspan</i>	1.00-1.50	m
<i>Average Chord</i>	0.21	m
<i>Aspect Ratio</i>	2.77	
<i>Flight Speed</i>	9.80-12.50	m/s

For our design, we identified the following eight requirements:

1. Flap wings of at least 0.20 m² surface area at 3.5 Hz. This requirement came by observing raven wings and was necessary to enable outdoor flight.

2. Flap each wing independently with the ability to synchronize wing motions when needed. This requirement was needed to perform normal flight and do aerobatics.
3. Have ability to program wing velocity and position as a function of time. This requirement was needed to optimize normal and aerobatic maneuvers.
4. Minimize weight to achieve flight and a climb rate of 0.5m/s.
5. Achieve minimum turning radius of 10 m. This requirement was needed to conduct tests in indoor stadiums and fly in outdoor fields with trees.
6. Remotely control the flight from a distance of 500 m.
7. Land unpowered at glide speed from a height of at least 3 meters without sustaining structural damage.
8. Demonstrate programmable wing kinematics with new maneuvers including dives, flips, steering and buttonhook turns.

2.2 System Decomposition

The identified design requirements for the Robo Raven led to a system decomposition containing the required major subsystems and the relationships among them, shown in Figure 1. This system decomposition was the basis for our component selection and integration, and led to the fuselage design required to support each subsystem.

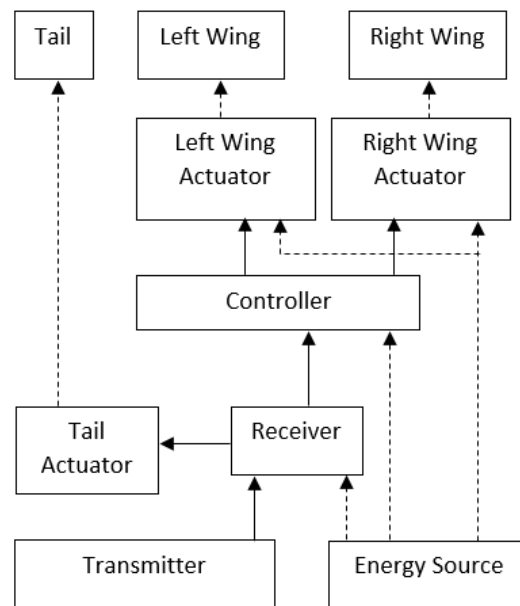


Figure 1 – Functional Decomposition of Robo Raven: Dotted lines (---) denote energy flows and solid lines (—) denote signal flows

Each system component was selected largely because it had the lightest weight of the available options while still meeting the system requirements, allowing maximized payload capacity². In addition to light weight, each component was chosen because of a small footprint, which was more suitable for mounting on the fuselage. The receiver was selected because it provided four channels to enable mapping of user inputs to desired aerobatic maneuvers. The Arduino Nano was also chosen because of its large number of input and output (I/O) pins (14 digital I/O pins and 8 analog inputs), required for processing signals for flight control, as well as its small size and low weight. The Futaba S9352HV servos are the heaviest part of the system at 68 grams each. Section 4 describes the rationale for their selection. The LiPo battery

² Disclaimer: any commercial product or company name in this paper is given for informational purposes only. Their use does not imply recommendation or endorsement by the U.S. Army Research Laboratory or the University of Maryland.

weighs 27 grams and was selected because it supports a very high discharge rate (20-40C rating), so it could accommodate the spikes in current draw of up to 7 amps. The interconnect wiring added another 19.8 grams. The weight is summarized in Table 2 below, along with the weight of the other non-electronic components.

Table 2 - Weight breakdown of Robo Raven for electronics, frame, wings, and tail, and total

Component	Weight (g)
Drive Actuators (2 - Futaba S9352HV)	136.0
Tail Actuator (Futaba S3114)	7.8
Controller (Arduino Nano)	6.0
Wiring	19.8
LiPo Battery	27.0
Spektrum 2.4 GHz Receiver	3.0
Wings (2)	26.0
Tail	8.0
Actuator Mount Assembly (for the S9352HV servos)	16.4
Frame	30.0
Foam Crash Protection	5.0
Assembly Fasteners	5.3
Total	290.3

3. Design and Fabrication of Wings

3.1 Wing Design

Wing design was adapted from a previously used approach developed in our lab for successfully realizing a FWAV platform with synchronized wing motion, which has been shown to be effective in generating lift and thrust forces across a variety of applications and size scales [14]. This design is shown in Figure 3. The parameters of the wing are as follows: S is the semi-span, C is the chord, and t_n are the diameters of carbon fiber stiffening rods. The wing membrane is a 0.001" thick film of biaxially-oriented polyethylene terephthalate (Mylar) which provides light weight, flexibility, and good toughness.

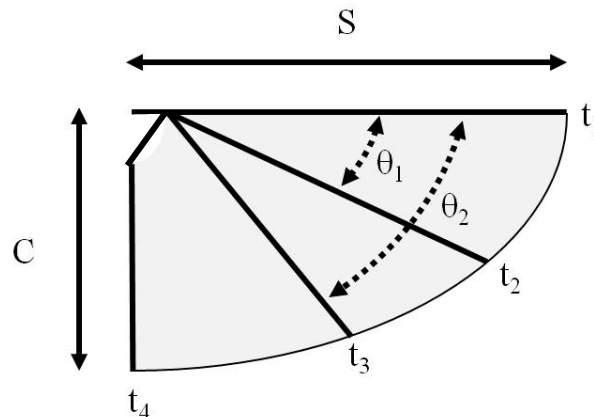


Figure 2 – Characteristic wing design: S is the semi-span, C is the chord, and t_n are the diameters of carbon fiber stiffening rods

Due to extensive usage of lightweight materials, this wing design changes shape passively in response to loads from the flapping motion. As the wings flap, aerodynamic loads on the compliant wing surface generate a significant camber change. The cambered wing is a thin airfoil, which captures and expels a large volume of air with each stroke. The induced shape change alternates with upstroke and downstroke producing lift and thrust. Since the wings are constructed with lightweight materials, they are easily deformed by aerodynamic loading, hence they are able to quickly reach an efficient shape to maximize force production throughout the flapping cycle. The selection of the design parameters shown in Figure 2 is very important because the stiffness distribution of the wing influences the shape that is induced by aerodynamic loads during flapping, which ultimately dictates whether forces are produced efficiently or not. This theme will be explored in greater detail in the remainder of this section.

3.2 Experimental Wing Design Procedure

The size of the wings and the flapping kinematics dictate the loading that is experienced during flapping. Based on results of experimental trials described in the Wing Drive Subsystem section, we established the angular velocity that corresponded to the highest power output from our drive motors.

We then took an experimental approach to wing characterization to find the best wing design by conducting a series of experiments with different wings. The objective of our experimental wing characterization was to select a wing geometry that would result in the servos operating as close as possible to their peak power operating condition.

Each wing design was evaluated using high speed video footage and a custom built test stand with a 6 degree of freedom load cell in a wind tunnel to measure the forces generated by the vehicle. The load cell used was an ATI Mini 40 Force Transducer, capable of measuring a maximum load of 40 N for thrust with a resolution of 1/100 N and a maximum load of 120 N for lift with a resolution of 1/50 N. A National Instruments PXI system was used to measure voltages from the load cell during wind tunnel testing, and these voltages were post-processed to obtain the lift and thrust forces. The test stand is shown in Figure 3. These tests were repeated under no air flow and significant air flow conditions with varying angle of attack. The load cell testing quantitatively revealed which wing created the most lift and thrust, while high speed video footage offered qualitative explanations for the results and provided design insight.

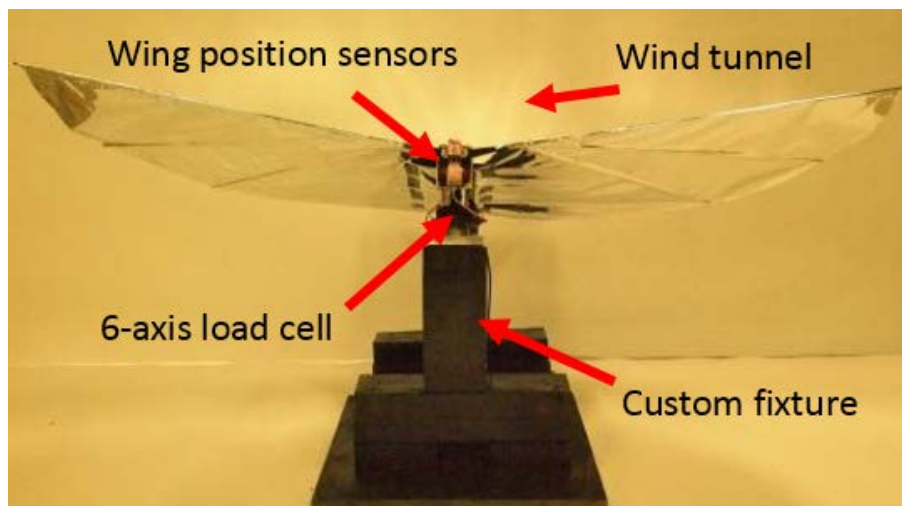


Figure 3 – Custom built test stand fixture with 6 DOF load cell in the wind tunnel.

We constructed and tested 18 different versions of the wing configuration using varying angles between spars, spar thicknesses, material thickness, and wing sizes.

Figure 4 shows images extracted from high speed footage of a wing as it goes through the flapping cycle. We measured curvature at various points on the wing as a function of time to ensure that the wing maintains the right curvature to ensure positive average lift under the appropriate airflow. Several beneficial properties are evident in the sequence of images shown. At the points where the wing is fully deformed, roughly corresponding to the middle of the upstroke and downstroke, the curvature is very smooth and does not exhibit discontinuities in curvature. In addition, there is a substantial amount of curvature which creates a large pocket in the middle of the span. This shape is characteristic of wings that produce very large thrust forces, while the absence of curvature discontinuities indicates a strong lift-producing wing [13]. Through this experimental process we converged on a wing design that reached the desired operating point for the selected actuators.

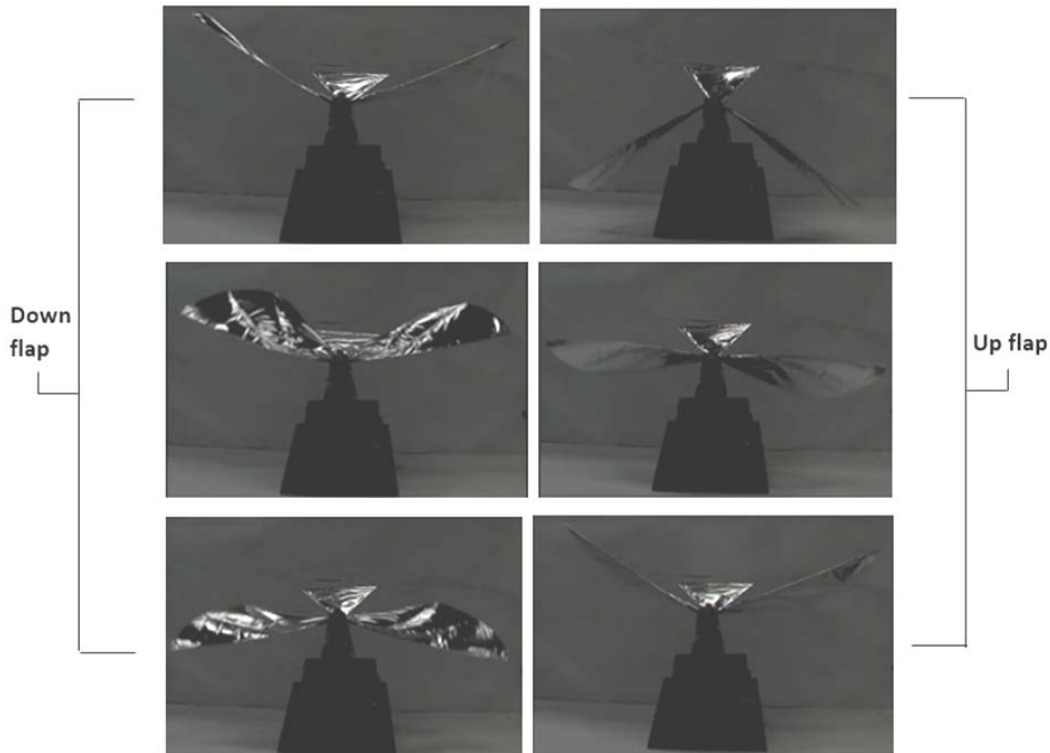


Figure 4 - High speed images of Robo Raven wing through one flap taken to evaluate wing shape deformation qualitatively.

3.3 Characterization of the Selected Wing Design

The experimentally designed wings were built by hand using a template matching the parameters in Table 3. Mylar was taped flat on a table and carbon fiber tubes were installed according to the template using Uhu Por® glue. Mylar strips were then used to cover and secure the carbon fiber stiffeners on the wing, and additional reinforcement Mylar was bonded to areas of higher stress concentrations to prevent tearing. Five holes were melted into the wing next to the chord-wise spar and number 8 rubber bands were tied through for tensioning the wing attachment to the frame. See Figure 5 for the completed wing. Based on our previous experiments, this manufacturing process has been shown to result in minimal variability across sets of wings [14].

These wings were tested in a wind tunnel (airspeed approximately 5 m/s) using the load cell test stand. The wings generated averages of 243 grams of lift and 120 grams of thrust at a 20 degree angle of attack. Lift and residual thrust data as a function of wing position from a sample trial are shown in Figure 6. Most of the lift is produced during the downward flap, while most of the thrust is produced during the upward flapping motion, a result that is expected and consistent with observations of flying animals [2].

The wings undergo significant deformations during the flapping cycle. Maintaining the right curvature is crucial from the aerodynamic lift production point of view. Our experiments revealed that any discontinuities in the curvature along the wing in either the chordwise or spanwise directions are likely to substantially degrade both lift and thrust performance, which need to be accounted for in the model. To ensure we were avoiding losses associated with shape discontinuities, we used digital image correlation (DIC) to precisely record the wings' translations and strains throughout the flapping cycle.

Table 3 – Wing Design Parameters

Parameter	Value	Units
S	605.8	mm
C	362.0	mm
t_1	3.18	mm
t_2	1.63	mm
t_3	1.63	mm
t_4	1.63	mm
θ_1	20	degrees
θ_2	40	degrees

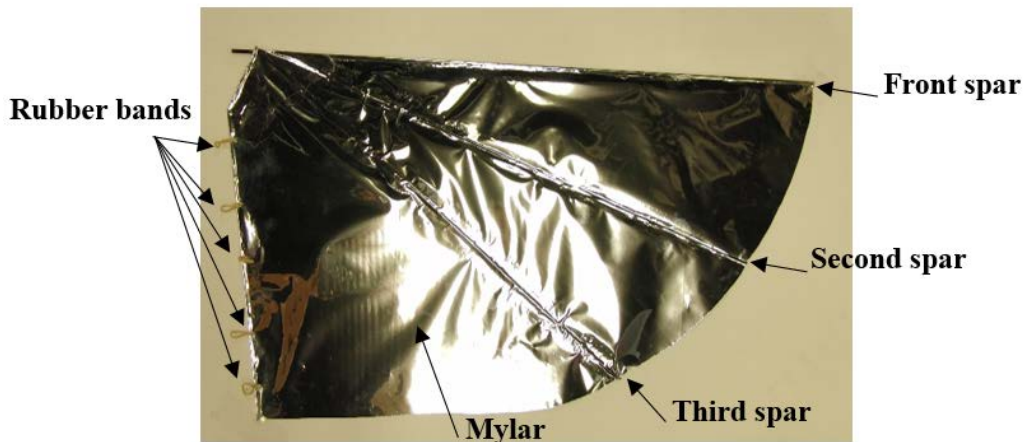


Figure 5 – Completed wing with geometry defined by Table 3

For DIC, two cameras are used to track a single object with a speckle pattern. The cameras used were two Flea 3 FW-03S1MC cameras. The cameras recorded a single wing flapping in the wind tunnel at 80 frames per second. The images were then processed using a VIC-3D from Correlated Solutions. This software takes the images with the speckle pattern and calculates the displacement and deformations along the speckled surface. DIC allowed us to ensure the wings had the right qualitative shapes during the flapping motion while also confirming the wing motions were accurately tracking the programmed gait kinematics.

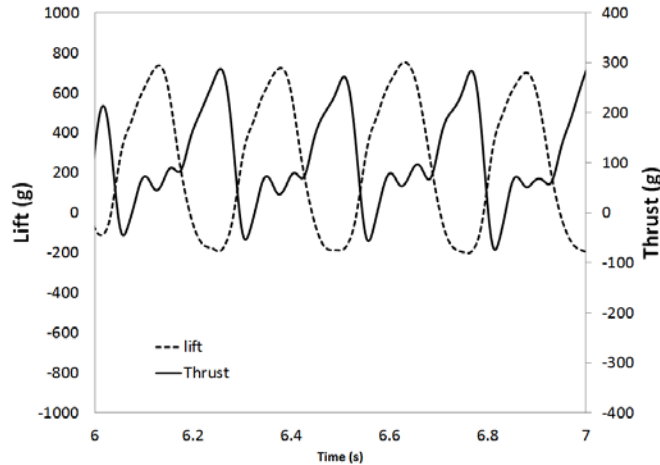


Figure 6 - Lift and thrust production during multiple flapping cycles

4. Design and Fabrication of Wing Drive Subsystem

The wing drive subsystem is responsible for producing the wingbeat kinematics that result in lift and thrust. Design of this subsystem is an important aspect of the vehicle design, therefore, we turned to nature for inspiration and to provide some insight into the trends that exist among feasible designs.

Power density is a key design factor for FWAVs to ensure lift and thrust forces are sufficient to overcome weight and drag. The design of custom actuators was beyond the scope of this effort, so we began by selecting a commercially available actuator for the wing drive subsystem. At this scale, electric motors are certainly the most popular actuator choice, but some alternatives exist. Popular choices include electrostatic actuators, bimetal bending actuators, piezoelectric cantilevers, shape memory alloys, and dielectric elastomers [22]. Our vehicle size limits our choices to the slower and more powerful actuators, including electric motors, shape memory alloys, bimetal benders, and dielectric elastomers. Of these choices, only electric motors and dielectric elastomers offer acceptably high efficiency of operation. However, the very high operating voltage presents integration challenges and required additional voltage step-up electronics on-board. Therefore, we decided to use brushless motors for our application.

Brushless motors must be paired with a flapping mechanism to provide reasonable speeds of operation. In addition, integration with a position sensor and a feedback loop is required for programmable kinematics. These requirements lead to increased weight, part count, complexity, and integration difficulty. To avoid the challenges associated with matching all of those components and designing the required hardware and software, we decided at an early stage in this effort to pursue servos for wing actuation, due to their high power output, programmable motions, and integrated packaging including the motor, drive train, speed controller, and position sensor.

Our approach of using a separate actuator for each wing increases weight relative to the traditional approaches of due to redundant mechanism parts and smaller, less efficient motors. For these reasons, we expected our available payload to be much smaller than would be possible with the coupled wing approach that we have explored in prior efforts. Light weight was a key requirement for all aspects of the design. Therefore, it was important to identify a servo that offered the most favorable combination of high power output and low total weight to maximize the likelihood of achieving flight in the prototype vehicle. In pursuit of this goal, we undertook a survey of available servos in a likely size range to identify a candidate for further testing.

The Futaba S9352HV was chosen due to its high figure of merit, computed as the power output divided by the mass. The available servos exhibit a linear relationship between available power and figure of

merit. While other servos exist on the market that offer either higher torque, higher speed, or lower mass, none are sufficiently strong performers in all three categories to justify their selection for our efforts.

We tested the S9352HV. The dynamometer and power analyzer together provided details about the electrical power input as well as the mechanical power output, from which we extracted the power and efficiency curves as a function of motor speed. Our objective was to determine the location of the power band, the operating condition that provided peak power output, and the operating condition that provided peak efficiency.

The results of our testing are summarized in Table 4. The maximum torque and speed are not reachable simultaneously. The peak power output of 9.4 Watts is reached at a final drive speed of about 8.9 rad/s which corresponds to approximately half the peak torque and speed.

Table 4 – Performance Test Results for Futaba S9352HV

	Value	Units
Stall Torque	12.5	mN-m
Top Speed	17.6	rad/s
Peak Power Output	9.4	W
Peak Efficiency	63.9	%
Mass	72	g

Due to the importance of weight minimization, we used 3D printing to manufacture the frame that comprised the primary structure of the vehicle. The ability to produce a part with complex geometry eliminated many assembly steps and hardware that would have otherwise been required. We sized the frame to minimize the weight and to ensure that it was capable of withstanding the expected load. The part is manufactured using ULTEM 9085 material [23], which has a tensile strength of 71.6 MPa. Our design has substantially less stress than this during normal operation. Iterative testing has shown that crashes imparting loads of over 5kg can be survived without part failure, yet the weight of the final part is only 8.0 grams.

The custom servo horns were laser cut out of 1/4" Delrin®. These servo horns fit over aluminum servo horns that physically attach to the servos and have 1/8" holes for the wings' front spars to fit into. To prevent off-axis loads from damaging the gear train inside each servo as well as to provide crash protection, a stiff 3D printed nose is attached to the front. Carbon fiber tubes are used to connect the front section to the tail and the rest of the body. An exploded view of the CAD model of the main drive system is shown in Figure 7 and the assembled vehicle is shown below in Figure 8.

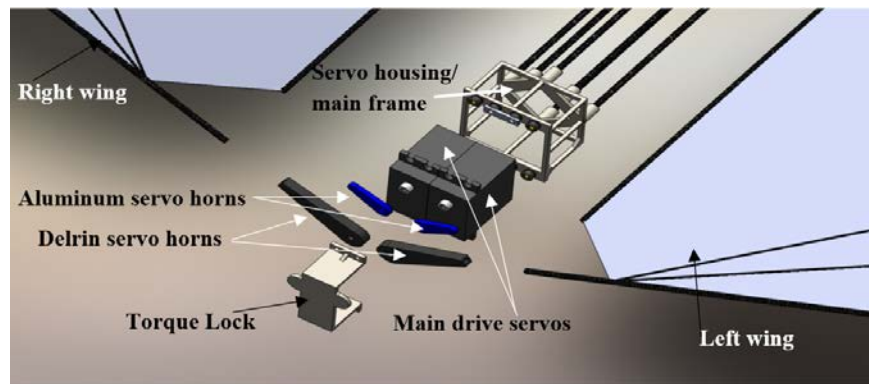


Figure 7 - Main drive assembly (exploded view)



Figure 8 – Main drive system assembled view

5. Design and Fabrication of Steering Subsystem

The Robo Raven was our first attempt at building a FWAV with independent wing control, and we expected to be able to steer by altering the flapping kinematics.

The thin airfoil theory has been used to describe many important factors relating to the functionality of birds' tails. A flat triangular tail may generate lift above angles of attack of 35 degrees, ideal for low speed flight. In addition, the sensitivity of the lift coefficient to angle of attack is low, further improving low speed maneuverability. With modification to the tail shape and orientation, the vertical flow over the tail surface may be altered, resulting in control and stability augmentation. For example, during a wing initiated roll, the tail may also be rolled to induce an asymmetry in its vortex structure. This leads to a stabilizing force that cancels the tendency for sideslip during a banked turn.

Our approach to the tail design is unconventional from a biological sense, due to the reversed angle of attack. Typically birds will only use a negative angle of attack during the approach to landing to generate a downward force, which rotates the nose of the bird upwards and retards forward speed. Then during the final approach to landing the tail and wings are both held at a large positive angle of attack to generate maximum lift. However, our design has a substantial amount of weight concentrated near the front due to the servos used for wing flapping, therefore, it is necessary to use a tail with a substantial negative angle of attack, which provides a strong nose-up moment that maintains balance. While this approach is less efficient due to the substantial component of induced drag, it is necessary to maintain stable flight. However, this configuration is conducive to low speed maneuvering due to the large coefficient of lift associated with high angles of attack.

We included a steering system consisting of a tail surface mounted to the rear of the fuselage. The tail maintains a fixed elevator angle while providing a variable roll angle relative to the fuselage. Due to weight restrictions, we were unable to add more than a single degree of freedom to the tail, a technique widely employed by birds [3]. However, the perfectly flat trailing edge is somewhat superior to many bird tails, which exhibit varying degrees of forkedness. A flat trailing edge allows for simplified manufacturing and is also an aerodynamically ideal solution. Any portion of the tail that contracts in span will be subject to the upstream wake and produce primarily drag, with a minimal contribution to lift. There are morphological constraints on birds that we need not abide by, so in this case we were able to implement a bioinspired design that provides an improvement over a biomimetic design.

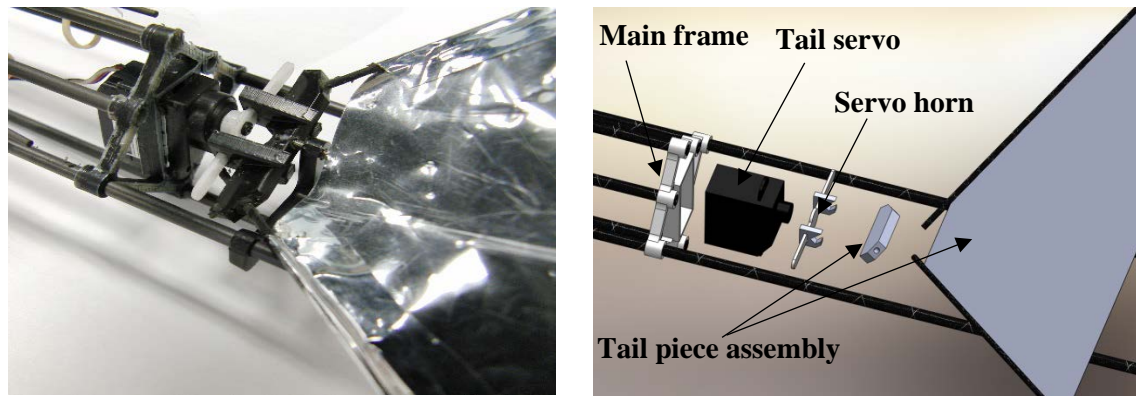


Figure 9 – Tail drive subsystem assembled (left) and exploded view (right)

Our design provides the option of fully controlling steering with the tail alone, or blending the steering control with wing motions to explore bio-inspired techniques of flight control. This enables us to execute aggressive maneuvers that will be described in more detail in Section 7. In addition, this layout gives us the ability to explore some behaviors that would be challenging or impossible to train an animal to execute, yet could still be informative from a research perspective. Figure 9 shows the assembled tail and an exploded view of all the components. Flight testing of this design revealed a minimum turn radius of 6 meters at a 40 degree tail angle, with an almost linear increase in turn radius proportional to reduced tail deflection. This leads to acceptable maneuverability with the tail alone to complete indoor flight tests in large buildings, and further enhancement through blended maneuvers that will be described in greater detail in section 8.

6. Design and Evaluation of Normal Flapping Gaits

The selection of a flapping gait requires the simultaneous selection of a number of important parameters including the flapping amplitude and rate, average dihedral, and periodic symmetry, among others. All of these parameters affect the flight speed and body pose, which significantly influence the forces produced during flight. Animals provide useful design insight in selecting a flapping gait due to broad similarities across many species. A survey of the locomotive properties of many animals provided a design goal based on the Strouhal number [25]. The Strouhal number describes the nature of vortex development and shedding for pitching and heaving airfoils, and is important in describing the propulsive efficiency of flapping wings [25]. Interestingly, there is a fairly narrow range of Strouhal number between 0.2 and 0.4 that many animals, including fliers and swimmers, operate in for efficient locomotion.

The Strouhal number is computed as the product of stroke frequency and amplitude, divided by flight speed. At this point, we only had knowledge about the angular velocity at which the motors develop maximum power, however we required additional information to proceed. Therefore, we sought to gain an understanding of the expected flight speed.

At a minimum, our objective with the Robo Raven would be to reach the lowest point on the P_{aero} curve, which corresponds to the minimum power required to sustain flight, and thus provides the greatest endurance. With any additional power leftover, we could then attempt to move farther left or right along the curve. Moving right would enable us to approach the most efficient flight speed, also referred to as the maximum range speed. At this point, a slightly higher power is required to sustain flight due to the increased profile power and parasite power needed, however there is a favorable tradeoff in terms of forward flight speed, allowing for an increased range for a given battery charge. In addition, slower flight speeds approaching hover may be realized by moving to the left along the power curve, which allows for greater maneuverability and smaller turn radii. However, this condition requires substantially more induced power, where the vehicle is held aloft almost entirely by thrust directed nearly downward.

Gerdes, J.W., Holness, A., Perez-Rosado, A., Roberts, L., Greisinger, A., Barnett, E., Kempny, J., Lingam, D., Yeh, C.H., Bruck, H.A., and Gupta, S.K., "Design, Manufacturing, and Testing of Robo Raven." Advanced Manufacturing Lab Technical Report, University of Maryland, College Park, April 2014.

Prior experiments revealed that when integrated into a flying prototype, this wing design will settle into a natural angle of attack and corresponding flight speed based on the weight distribution of the vehicle [11, 13]. The exact angle of attack is difficult to exactly predict ahead of time, however the forces generated during flapping are highly sensitive to this parameter. Testing indicated that the velocity for minimum power is typically reached around a 20 degree angle of attack, therefore we proceeded using this assumption.

We used the prototype vehicle shown in Figure 10 for flight testing. Initially, the angle of attack required adjustment, as early flights exhibited a very high forward speed and gradual loss of altitude. This was likely due to the large concentration of weight at the front attributed to the servos. Therefore, a small extension was added to the rear of the fuselage from which the battery was suspended, which shifted the center of mass aft, and thus the angle of attack increased, directing the net force vector closer to vertical. We also adjusted the gait by increasing the flapping amplitude and slightly increasing the flapping rate, and following the methods of [25], we found our Strouhal number with the gait adjustments to be 0.395. This brought our prototype within the range commonly exhibited by flying animals, and resulted in sustained flight with the ability to climb and maneuver.



Figure 10 - Fully Assembled Robo Raven (left) and CAD version (right)

The flapping gait was programmed on the Arduino Nano. Average force production during testing was 242.9 g (5.5 s.d.) lift and 119.6 g (6.4 s.d.) thrust. Due to some turbulence in the wind tunnel a small amount of variability was present across trials. The typical flight duration of the system with a 370 mAh onboard LiPo battery is 4 minutes and 45 seconds.

Flight testing the Robo Raven has helped us to understand the capabilities and operational conditions during cruising, which are summarized in Table 5. Comparison of these results with flying ravens and observation of the flight dynamics reveals we are likely operating near the low-speed, minimum-power flight condition, as shown by the relatively large 20 degree angle of attack. This comes from the limitation on available power from the motors, combined with the weight of the prototype that approaches the limit of at which it will fly. With some additional power or weight savings, it is expected that the flight envelope will broaden to include faster more efficient flight, as well as slower flight approaching hover. The angle of attack was verified in two ways, first by taking screenshots from high speed video during free flight we measured the average vehicle attitude. Then, we confirmed the measurement with wind tunnel testing at increasing angles of attack until the residual thrust-drag component vanished, indicating we had reached the flight equilibrium condition. Both measurements were in agreement on the 20 degree value.

Table 5 – Flight test results of the Robo Raven

Parameter	Value	Units
<i>Flap Rate</i>	4.0	Hz
<i>Flap Amplitude</i>	100	degrees
<i>Angle of Attack</i>	20	degrees
<i>Climb Rate</i>	0.53	m/s
<i>Reynolds Number</i>	124,000	-
<i>Strouhal Number</i>	0.395	-
<i>Minimum Turning radius</i>	6.1	m

7. Design and Evaluation of Aerobatics Maneuvers

Our goal was to duplicate some of the impressive behaviors that have been observed by Ravens [26-28, 21]. It was not possible for us to exactly reproduce flight dynamics of Ravens because of limited degrees of freedom in Robo Raven. So we focused on functionally reproducing selected aerobatics.

Aggressive maneuvers like buttonhook turns may be executed by banking the FWAV as shown in Figure 11. This maneuver is initiated by commanding one wing to move to a 40 degree dihedral and the other to move to a 40 degree anhedral. This rotates the frame, resulting in enhanced tail rotation and a stronger turn than would be possible with just rotating the tail. Combined wing and tail turning modes result in a 90 degree tail rotation relative to the fuselage. Combined with the ceased flapping, this motion sequence sends the bird into an extremely tight turn. Flapping is resumed to continue flying after the motion is completed. The maneuver allows for a turning radius of 2.4 meters which is significantly smaller than the tail-based minimum turning radius of 6 m. It takes 2.1 seconds to complete a full 180 degree turn with this control, and Robo Raven drops about 3 meters during the turn. This altitude loss is expected due to the lost lift and thrust associated with non-flapping wings.

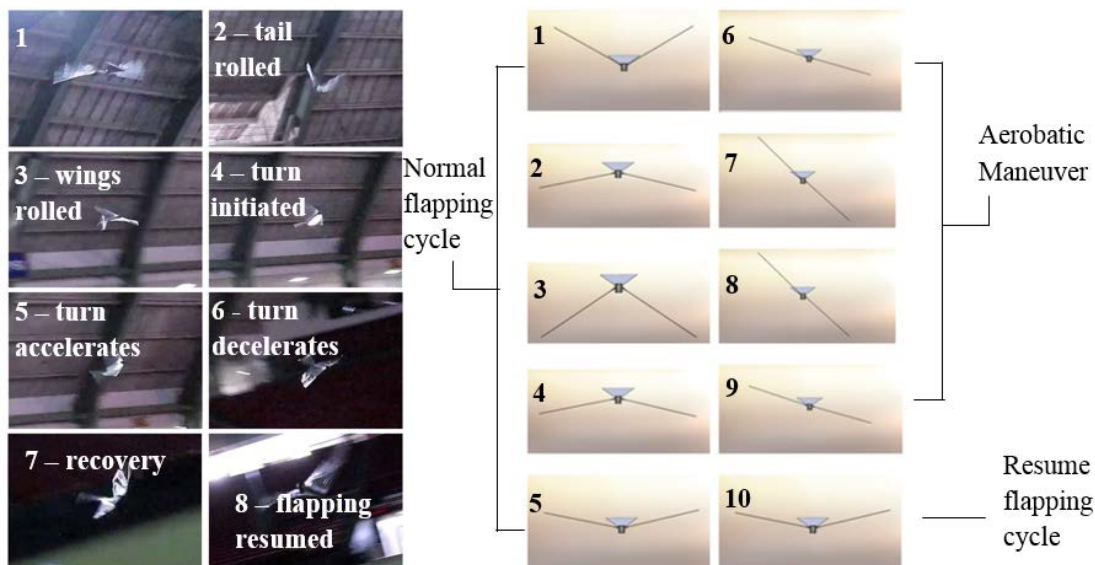


Figure 11 - Buttonhook turn maneuver (left) and CAD representation of motion sequence (right)

Another maneuver we explored was the back flip shown in Figure 12, which is a step toward developing a pre-landing flare maneuver or an obstacle avoidance strategy. This aerobatic maneuver is initiated by commanding both wings to rapidly move below the fuselage which initiates the backwards roll. Moving the center of lift below the center of mass creates a force imbalance, aided by the drag of the elevated tail surface, both of which further accelerate the roll. Flapping resumes to continue flying after the motion is completed. This maneuver takes 1.7 seconds to complete. This number will change as the inclined angle of each wing varies from 40 degrees as the inclined angle will determine the amount the bird “throws” itself into the backflip, and will change the effective surface area for drag calculations which will reduce the forward velocity when the bird is vertical during the flip.

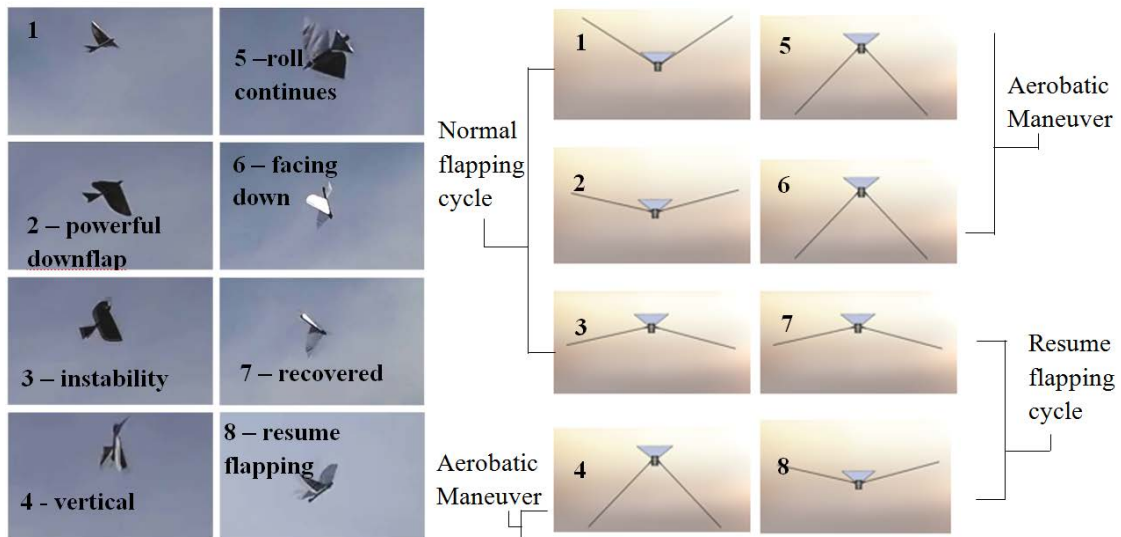


Figure 12 – Back flip maneuver (left) and CAD representation of motion sequence (right)

The third maneuver we tested was a dive motion, shown in Figure 13. This maneuver was initiated by moving both wings to a 40 degree dihedral and holding for as long as the dive command is received. The bird is well balanced when in this position so that it simply drops and does not flip or otherwise change its orientation. During the dive motion, airspeed is greatly increased, reminiscent of an attacking bird of prey. Flapping is resumed at the end of the motion to allow recovery and continued flight.

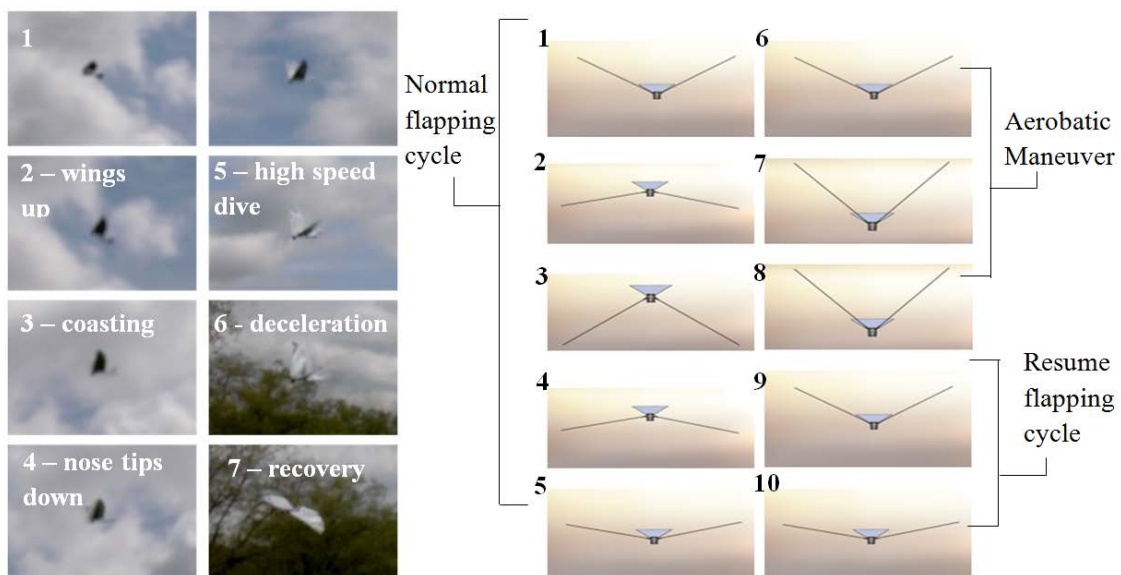


Figure 13 – Dive maneuver (left) and CAD representation of the motion sequence (right)

Videos of these motions and the Robo Raven flying can be found on YouTube at the following links:

“Robo Raven” <http://www.youtube.com/watch?v=mjOWpwbnmTw>

“Robo Raven Twins Learning Aerobatics!” <http://www.youtube.com/watch?v=XhsXul39DZg>

8. Conclusions

We have developed a new FWAV platform called Robo Raven that flies with independently controlled wings powered by digital servo motors. This increases flight control capability and takes us a step closer to the real capability of birds. Thus, this platform represents a significant advance towards biomimicry of birds in FWAV platforms and the subsequent flight capabilities that it enables.

Successfully realizing this platform required a multi-faceted approach. First, we used advanced manufacturing processes such as 3D printing and laser cutting to create lightweight polymer parts to reduce the weight. Second, we programmed wing motion profiles that ensured that wings maintain the optimal velocity during the flap cycle to achieve the right balance between the lift and the thrust. Third, we developed a method to measure aerodynamic forces generated during the flapping cycle. This enabled us to quickly evaluate many different wing designs to select the best one. Finally, we adopted a systems approach to make sure that all components worked well as an integrated system.

While inspiration from birds was useful in helping to arrive at a flying prototype, there are still key differences between flying animals and Robo Raven. The wings used on Robo Raven are extremely thin relative to a bird's, and still have fewer degrees of freedom due to our choice of a single actuator per wing for actuation. Robo Raven's wings also lack the fine control over feathers possessed by birds, and the twist dynamics are a passive function of the forces imposed on them as opposed to a multiple DOF system as in birds. Additional discrepancies include a less than optimal body design, which lacks the benefits of a lifting body that many birds take advantage of. Despite these important differences, several similarities were found between the flight characteristics of Robo Raven and flying animals of a similar size range.

This effort will allow FWAVs to take advantage of the variety of flight styles that birds have, which will allow for tailoring of flights to better accomplish mission objectives. This can be based on a detailed understanding of how the motor, wings, and flapping gait will respond to changes in their respective operating conditions. Finally, the capabilities of using Robo Raven to explore expanded maneuvering capabilities afforded by independently controllable wings was demonstrated, which should lead to new modes of flight for FWAVs and expand their usefulness in the rapidly growing UAV marketplace.

Acknowledgement: This work was sponsored by U.S. Army Research Laboratory Vehicle Technologies Directorate and the Science, Mathematics, & Research for Transformation Scholarship, administered by the American Society for Engineering Education and Naval Postgraduate School. The support of AFOSR grant FA9550-12-1-0158, Dr. Byung-Lip “Les” Lee program manager, is also greatly appreciated.

References

- [1] A. Azuma, *The Biokinetics of Flying and Swimming*, 2006.
- [2] U. M. Norberg, *Vertebrate Flight* vol. 27. New York: Springer-Verlag, 1990.
- [3] J. J. Videler, *Avian Flight*: Oxford Ornithology Series, 2005.
- [4] M. H. Dickinson, F. Lehmann, S. Sane, "Wing Rotation and the Aerodynamic Basis of Insect Flight," *Science*, vol. 284, pp. 1954-1960, 1999.

- [5] L. Demasi, A. Palazotto, A. Hollenbeck, R. Cavallaro, "Exploratory Structural Investigation of a Hawkmoth-Inspired MAV's Thorax," in *53rd AIAA/ASME/ASCE/AHS/ASC Structures, Structural Dynamics and Materials Conference*, Honolulu, Hawaii, 2012.
- [6] D. K. Riskin, J. Iriarte-Diaz, KM Middleton, SM Swartz. "The effect of body size on the wing movements of pteropodid bats, with insights into thrust and lift production," *The Journal of Experimental Biology*, pp. 2110-2122, 2010.
- [7] G. Bunget and S. Seelecke, "BATMAV: a biologically inspired micro air vehicle for flapping flight kinematic modeling," in *Proc. SPIE 6928, Active and Passive Smart Structures and Integrated Systems*, 2008.
- [8] J. J. Videler, *Avian Flight*. Oxford: Oxford University Press 2005.
- [9] W. Bejgerowski, A. Ananthanarayanan, D. Mueller, S. K. Gupta, "Integrated product and process design for a flapping wing drive mechanism," *Journal of Mechanical Design*, vol. 131, pp. 061006-1, 2009.
- [10] W. Bejgerowski, J. W. Gerdes, H. A. Bruck, S. K. Gupta, "Design and fabrication of miniature compliant hinges for multi-material compliant mechanisms," *International Journal of Advanced Manufacturing Technology*, vol. 57, pp. 437-452, 2011.
- [11] K. Cellon, "Characterization of flexible flapping wings and the effects of solar cells for miniature air vehicles," MS, Mechanical Engineering, University of Maryland, College Park, 2010.
- [12] D. Mueller, J. W. Gerdes, S. K. Gupta, "Incorporation of passive wing folding in flapping wing miniature air vehicles," *ASME Mechanism and Robotics Conference*, e San Diego, CA, 2009.
- [13] J. W. Gerdes, "Design, analysis, and testing of a flapping-wing miniature air vehicle," MS, Mechanical engineering, University of Maryland, College Park, 2010.
- [14] J. W. Gerdes, K. Cellon, H. A. Bruck, S. K. Gupta, "Characterization of the mechanics of compliant wing designs for flapping-wing miniature air vehicles," *Experimental Mechanics*, vol. 53, pp. 1561-1571, 2013.
- [15] J. W. Gerdes, L. Roberts, A. Perez-Rosado, E. Barnett, J. Kempny, H. A. Bruck, S. K. Gupta, "Wing performance characterization for flapping wing air vehicles," *ASME Mechanism and Robotics Conference*, Portland, Oregon, 2013..
- [16] D. Mueller, H. A. Bruck, S. K. Gupta, "Measurement of Thrust and Lift Forces Associated With Drag of Compliant Flapping Wing for Micro Air Vehicles Using a New Test Stand Design," *Experimental Mechanics*, vol. 50, pp. 725-735, 2009.
- [17] J. W. Gerdes, S. Wilkerson, S. K. Gupta, "A Review of Bird-Inspired Flapping Wing Miniature Air Vehicle Designs," *Journal of Mechanisms and Robotics*, vol. 4, pp. 021003-1, 2012.
- [18] W. Bejgerowski, J.W. Gerdes, S. K. Gupta, H. A. Bruck, and S. Wilkerson. Design and fabrication of a multi-material compliant flapping wing drive mechanism for miniature air vehicles. *ASME Mechanism and Robotics Conference*, Montreal, Canada, August 2010.
- [19] A. Perez-Rosado, A. Philipps, E. Barnett, L. Roberts, J. W. Gerdes, S. K. Gupta, and H. A. Bruck. Compliant multifunctional wing structures for flapping wing MAVs. *SEM Annual Conference and Exposition*, Lombard, IL, 2013.
- [20] A. Ananthanarayanan, W. Bejgerowski, D. Mueller and S. K. Gupta. Development of a multi-piece multi-gate mold for manufacturing a flapping wing drive-mechanism. *North American Manufacturing Research Conference*, Monterrey, Mexico, May 2008.

- [21] P. Zoo. (12 August 2013). *Common Raven*. Available: http://www.phoenixzoo.org/visit/animal_news.aspx?ARTICLE_ID=100564
- [22] M. Karpelson, J. Whitney, W. Gu-Yeon, R. Wood, "Energetics of Flapping-Wing Robotic Insects: Towards Autonomous Hovering Flight," in *Intelligent Robots and Systems (IROS), 2010 IEEE/RSJ International Conference on*, 2010, pp. 1630-1637.
- [23] Stratasys. (21 November 2013). *ULTEM 9085 Spec Sheet*. Available: <http://www.stratasys.com/materials/fdm/ultem-9085>
- [24] G. K. Taylor, R. Nudds, A. Thomas, "Flying and swimming animals cruise at a Strouhal number tuned for high power efficiency," *Nature*, vol. 425, pp. 707-711, 2003.
- [25] J. M. Anderson, K. Streitlien, D. Barrett, M. Triantafyllou, "Oscillating foils of high propulsive efficiency," *Journal of Fluid Mechanics*, vol. 360, pp. 41-72, 1998.
- [26] B. Heinrich, *Mind of the raven: investigations and adventures with wolf-birds*. New York: HarperCollins Publishers Inc, 1999.
- [27] Nature. (12 August 2013). *Ravens*. Available: <http://www.pbs.org/wnet/nature/episodes/ravens/introduction/1506/>
- [28] National Geographic. (15 August 2013). *Common Raven*. Available: <http://animals.nationalgeographic.com/animals/birding/common-raven/>